Triple Ion-Beam Studies of Radiation Damage Effects in a 316LN Austenitic Alloy for a High Power Spallation Neutron Source

E. H. Lee, G. R. Rao, J. D. Hunn, P. M. Rice, M. B. Lewis,
S. W. Cook, K. Farrell, and L. K. Mansur
Metals and Ceramics Division
Oak Ridge National Laboratory
P.O. Box 2008
Oak Ridge, TN 37831-6376, USA

Abstract

Austenitic 316LN alloy was ion-irradiated using the unique Triple Ion Beam Facility (TIF) at ORNL to investigate radiation damage effects relevant to spallation neutron sources. The TIF was used to simulate significant features of GeV proton irradiation effects in spallation neutron source target materials by producing displacement damage while simultaneously injecting helium and hydrogen at appropriately high gas/dpa ratios. Irradiations were carried out at 80, 200, and 350°C using 3.5 MeV Fe^{++}, 360 keV He^{+}, and 180 keV H^{+} to accumulate 50 dpa by Fe, 10,000 appm of He, and 50,000 appm of H. Irradiations were also carried out at 200°C in single and dual ion beam modes. The specific ion energies were chosen to maximize the damage and the gas accumulation at a depth of ~ 1μm. Variations in microstructure and hardness of irradiated specimens were studied using transmission electron microscopy (TEM) and a nanoindentation technique, respectively. TEM investigation yielded varying damage defect microstructures, comprising black dots, faulted and unfaulted loops, and a high number density of fine bubbles (typically less than 1 nm in diameter). With increasing temperature, faulted loops had a tendency to unfault, and bubble microstructure changed from a bimodal size distribution to a unimodal distribution. Triple ion irradiations at the three temperatures resulted in similar increases in hardness of approximately a factor of two. Individually, Fe and He ions resulted in a similar magnitude of hardness increase, whereas H ions showed only a very small effect. The present study has yielded microstructural information relevant to spallation neutron source conditions and indicates that the most important concern may be radiation induced hardening and associated ductility loss.

Introduction

The National Spallation Neutron Source (NSNS) development effort calls for the planning and construction of an accelerator-based spallation neutron source facility, operating at approximately 1 MW and ungradable later to 2 and 5 MW [1,2]. In such a system, materials surrounding the mercury target will be exposed to a high flux of 1 GeV protons in a pulsed mode, as well as substantial neutron flux, including neutrons with energies from the proton energy down to thermal energies. The operating temperature is expected to be below 200°C. In the NSNS environment, it is anticipated that atomic displacement rates will be high, up to ~10^{-2} dpa/s during the microsecond beam pulse period, with a 30-60 Hz pulse frequency. In addition, considerable quantities of transmutation products, particularly hydrogen and helium, will be generated at a rate of up to ~200 appm He/dpa and ~1000 appm H/dpa, respectively . In such a radiation environment, materials will suffer severe damage. Typically, for metal alloys subjected to radiation, tensile strength increases, ductility decreases, toughness decreases, and geometrical dimensions change due to radiation induced hardening, solute segregation, gas bubble formation, swelling, and creep. Data for the evaluation of acceptable lifetimes of the planned NSNS system under such a demanding radiation environment are urgently needed.

Although considerable data have been generated in the past for fission reactor environments, there is very little available information and limited experience with materials' performance under spallation source irradiation conditions. For the initial stage of spallation source development, data from fission reactor experiments as well as from accelerator simulations will need to be used. As part of the accelerator simulations, irradiation experiments have been carried out using the Triple Ion-beam Facility (TIF) at Oak Ridge National Laboratory (ORNL). This facility can be used to simulate the NSNS irradiation environment by producing displacement damage in candidate materials while simultaneously injecting H and He. Currently, austenitic and ferritic steels are the major potential candidate structural materials for the mercury target container. Since austenitic stainless steel has good toughness at low temperatures, it is the primary choice for the target structural material and is the subject of this investigation. Irradiations were carried out at a continuous damage rate of ~10^{-3} dpa/s, about an order of magnitude lower than the NSNS irradiation environment during the beam pulse period. Microstructures of irradiated specimens were examined by transmission electron microscopy (TEM), and hardening was investigated using a nanoindentation technique. Irradiation of ferritic steel is also in progress and results of that study will be reported separately.

Experimental Procedures

Details regarding the triple ion beam facility can be found in Ref. [3]. Table I lists the composition of the austenitic 316LN stainless steel alloy investigated in this work. The material was solution annealed at 950°C for 2 hours in vacuum (~10^{-4} Pa). Solution annealed and electrochemically polished 3 mm diameter TEM disk specimens were irradiated in triple, dual, and single ion beam modes. It should be noted that the irradiations were carried out in a non-pulsed mode. The irradiation conditions were chosen so that the deposition range of He and H gas overlapped the Fe^{++} peak damage region by using the Monte Carlo simulation code The Stopping and Range of Ions in Matter (SRIM, 1996 version, formerly known as TRIM) [4]. A displacement threshold energy of 40 eV was used for the calculations [5]. Figure 1 compares SRIM calculated vacancy distribution (vacancies/ion/nm) as a function of depth for 3.5 MeV Fe^{++}, 360 keV He^{+}, and 180 keV H^{+}, which were the ion energies used in this study.

The NSNS materials' irradiation simulation experiments are still in progress. The matrix of irradiation conditions and the experiments completed are shown in Table II. This paper summarizes the results obtained thus far. For the irradiations, a total Fe^{++} fluence of $5x10^{20}$ ions/m^2 was employed to accumulate 50 dpa at the peak damage depth of approximately 1 μm. The contributions of He and H to the

Lee1

DISCLAIMER

Table I Composition of 316LN Austenitic Alloy in Weight Percent (%)

Fe	Ni	Cr	Mo	Mn	Si	C	N
Bal	12.3	17.4	2.3	1.8	0.46	0.02	0.06

Table II Irradiation and Materials Characterization Test Matrix

Temperature (°C)	3.5 MeV Fe^{++}, 360 keV He^{+}, 180 keV H^{+}						
	Fe^{++}+He^{+} +H^{+}	Fe^{++} +He^{+}	Fe^{++} +H^{+}	Fe^{++}	He^{+} +H^{+}	He^{+}	H^{+}
80	•						
200	•	•	•	•	•	•	•
350	•						

displacement damage were 0.9 and 0.3 dpa respectively. The ion irradiation rates ranged from $1x10^{-3}$ to $3x10^{-3}$ dpa/s for the triple ion irradiations, which are about an order of magnitude lower than the displacement damage rates expected in the NSNS when the beam is on target. The peak injection rates of helium and hydrogen according to SRIM were ~200 appm He/dpa (0.5-1.5 appm He/s) and ~1000 appm H/dpa (3-8 appm H/s) to accumulate 10,000 appm He ($3.5x10^{20}$ ions/m^2) and 50,000 appm H ($1.4x10^{21}$) ions/m^2 at the peak damage depth, respectively. The irradiations were conducted at ~80°C (caused by beam heating from room temperature), 200°C and 350°C.

Hardness changes in the materials were measured using a nanoindentation hardness tester which uses a pyramidal Berkovich indenter. Hardness data were obtained by indenting normal to the ion-irradiated surface to a total depth of 700 nm. Since the thickness of the ion-beam modified layer is very shallow, in the range of 1 μm, the effect of the underlying unirradiated substrate becomes significant as the indenter approaches the depth of the ion range. At shallow surface depths less than 50 nm, measured hardness values are unreliable because of uncertainties in the tip geometry of the indenter and other surface artifacts such as an oxide layer and polishing defects. In this report, it was found that the hardness value at 200 nm indentation depth is a good representation of the surface hardness for comparison purposes with the least surface and substrate effects as described in the results section. Details about the procedure for the hardness measurement are described elsewhere [6,7]. The elastic effects from both the modified layer and the supporting materials have been discussed by Bhattacharya and Nix [8]. To accommodate the effects of the substrate, indenter tip geometry, and other subsurface artifacts, hardness values can be normalized to the unirradiated material hardness.

Transmission electron microscopy (TEM) specimens were prepared by electrochemically removing a 600-700 nm surface layer from the ion bombarded side. The specimens were then backthinned from the unirradiated side until perforation, such that the perforation was close to the peak damage region, as indicated by the two vertical lines in Figure 1. The thinned specimens were examined in a Phillips CM-12 electron microscope operated at 120 keV.

Results

TEM examination of triple ion irradiated specimens revealed that the displacement damage induced defects mostly comprise black dots, faulted loops, and an extremely high number density of bubbles (~10^{25}/m^3). Although faulted loops tended to unfault to form prismatic loops progressively with increasing irradiation temperature from 80 to 350 °C, very few network dislocations were observed even at 350°C. Thus the overall point defect sink strength stayed about the same at all three temperatures. Figure 2 compares TEM microstructures of unirradiated and irradiated specimens for 80, 200, and 350°C irradiations. The apparent variations in dislocation densities in the micrographs are mainly due to variations in the TEM specimen foil thickness. The observed defect types are summarized in Table III. Although defect microstructure varied somewhat as a function of temperature, overall dislocation densities were estimated to be in the 10^{13} -10^{14} m/m^3 range at all three temperatures. Very few dislocations could be imaged for the unirradiated alloy at high TEM magnifications. Typical dislocation density for a well-solution-annealed alloy is generally less than 10^{12} m/m^3.

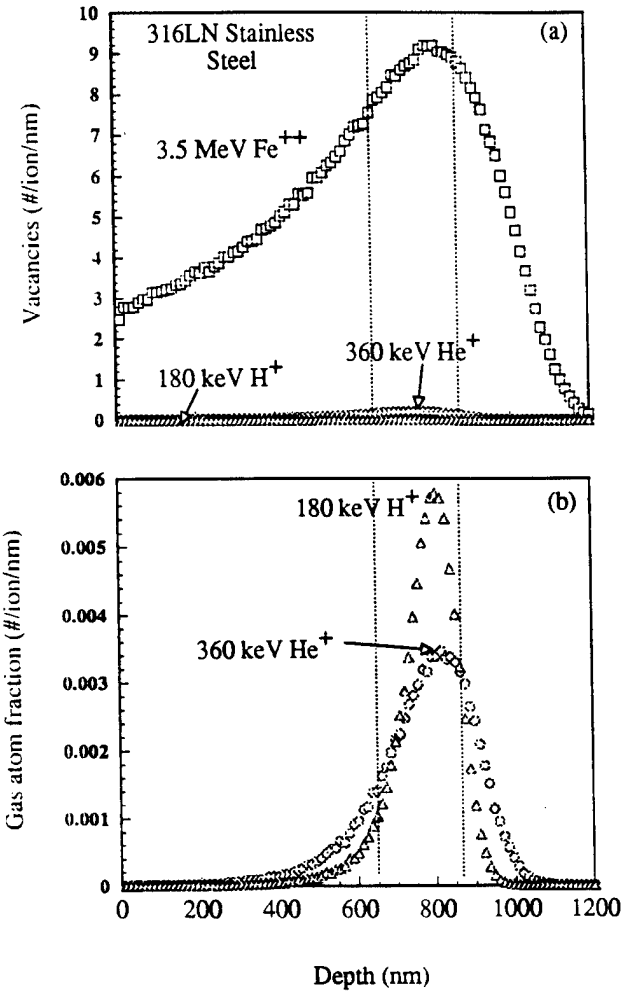

Figure 1. SRIM calculated average damage values per unit length caused by one ion for irradiation using 3.5 MeV Fe^{++}, 360 keV He^{+} and 180 keV H^{+} (a) and fractional gas atom distribution for one gas atom (b).

Most bubbles were very small, less than a nanometer in diameter, so that they could not be imaged clearly even at high magnifications. When helium concentration levels are very high, it is often possible to estimate bubble number density by deriving the helium bubble lattice parameters from TEM diffraction spots [9]. Such diffraction spots were not observed in this work because the helium concentration levels were not high enough to produce a bubble lattice. Therefore, the less accurate thickness fringe method was employed to estimate foil thickness and bubble number density. Difficulty in imaging the small sized bubbles and errors in foil thickness measurements made the bubble counting inaccurate. With a probable error of a factor of 2, the bubble number density was estimated to be in the range of ~$4x10^{25}$/m^3;

Lee 2

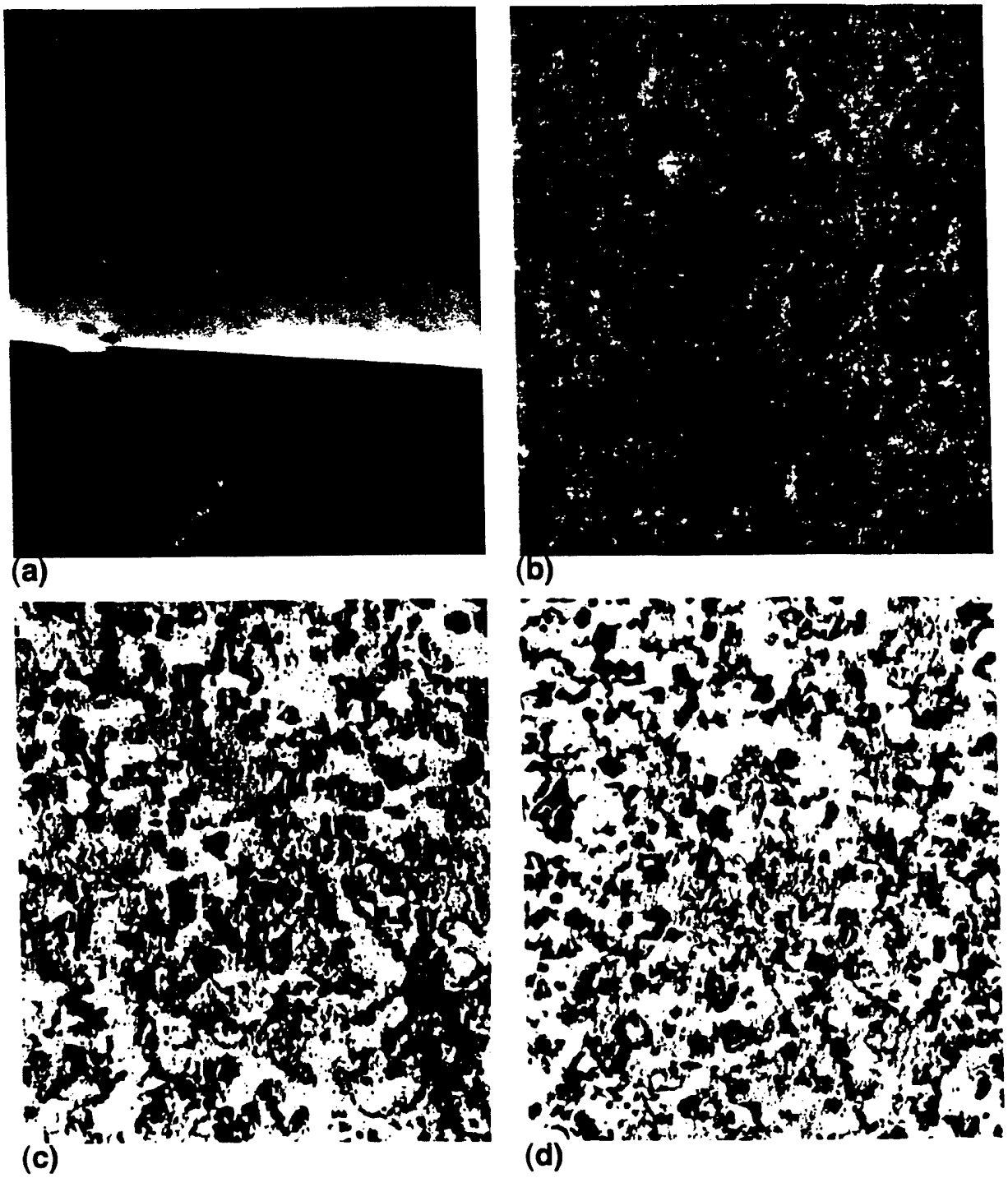

Figure 2: TEM microstructures of (a) unirradiated and triple ion irradiated specimens irradiated at (b) 80°C, (c) 200°C and (d) 350°C.

Table III Temperature Dependence of Dislocation and Bubble Microstructure

4 MeV Fe^{++}, 400 keV He^{+}, 200 keV H^{+} Triple Beam Irradiations		
80°C	200°C	350°C
black dots faulted loops (30~70 nm) bimodal bubble size distribution	black dots unfaulted loops (~20 nm) unimodal bubble size distribution	black dots unfaulted loops some line segments unimodal bubble size distribution

~$2.5 \times 10^{25}/m^3$, and ~$1.5 \times 10^{25}/m^3$ for 80, 200, and 350°C, respectively. Figure 3 compares the bubble microstructures of 80, 200 and 350°C irradiated specimens at a high magnification. The micrographs shown were taken in a slightly underfocused condition and it was verified that the observed features were indeed bubbles by using the standard procedure of observing the change in contrast while underfocusing and overfocusing. Surprisingly, a bimodal bubble size distribution was observed at 80°C, with larger bubbles than those observed at 350°C. At 350°C, bubble distribution was essentially unimodal with very few large bubbles.

TEM microstructures for single, dual, and triple ion irradiated specimens, all irradiated at 200°C are compared in Figure 4. The displacement damage levels for 3.5 MeV Fe^{++}, 360 keV He^{+}, and 180 keV H^{+} irradiated to the doses mentioned are 50 dpa, 0.9 dpa and 0.3 dpa, respectively. Predominant defect types varied with ion species as summarized in Table IV. Single H^{+} beam irradiation produced the finest black dots and bubbles, mostly much smaller than one nanometer, which is close to the TEM resolution limit. Single He^{+} ion beam irradiation produced small loops (~10 nm) in addition to black dots and bubbles. Single Fe^{++} ion beam irradiation produced somewhat larger loops (~50 nm) in addition to black dots but no discernible bubbles. The dual beam results show that H^{+} irradiation resulted in finer loop sizes, while He^{+} ions caused coarsening of the loop size. Most refinement of loop size occurred when both H^{+} and He^{+} ions were used, as demonstrated for the triple beam irradiation, Figure 4.

Hardness values are shown in Figure 5 as a function of indentation depth for *control* and *triple* ion beam irradiated specimens for 80, 200, and 350°C irradiations. It should be noted that the error range for the hardness measurements was ±0.25 GPa. The hardness values at 200 nm indentation depth increased by almost a factor of 2 after irradiation, from ~3 GPa to ~5.8 GPa. It is interesting to note that the hardness change was insensitive to irradiation temperature. Figure 6 shows hardness values of the irradiated specimens normalized to the unirradiated specimen hardness value. Hardness ratios were found to be approximately two for all three temperatures. A gradual decrease in hardness ratio was evident beyond 200 nm indentation depth caused by greater influence of the underlying unirradiated substrate. Typically, the stress field surrounding the indenter tip extends to about 7 times the penetration depth. Thus hardness values at 200 nm depth have been used as representative values for comparison in this report.

Figure 7 compares hardness data for single, dual, and triple ion beam irradiated specimens, all irradiated at 200°C. *Triple* Fe^{++}+He^{+}+H^{+} beam produced the highest increase in hardness (~5.8 GPa) followed by *dual* Fe^{++}+He^{+} beam (~5.3 GPa at 200 nm depth), indicating that H^{+} contributed slightly to the extent of about 0.5 GPa. This is confirmed when unirradiated and H^{+} ion irradiated specimens are compared in Figure 7. On the other hand, interestingly, both single Fe^{++} and single He^{+} irradiations produced a similar magnitude of increase in hardness, from ~3 GPa for the unirradiated material to ~4.3 GPa at 200 nm depth, whether H^{+} ions were simultaneously injected or not, hinting that the effect of H^{+} effect was minimal and subtle.

Discussion

TEM microstructural examination and hardness measurements were carried out for 316LN austenitic alloy irradiated with 3.5 MeV Fe^{++} (50 dpa), 360 keV He^{+} (10,000 appm), and 180 keV H^{+} (50,000 appm) ion beams. The triple ion beam irradiation results at 200 °C showed that hardness values at 200 nm indentation depth increased from approximately 3 GPa for the control specimen to ~5.8 GPa after irradiation. A similar magnitude of increase in radiation-induced hardening occurred for 80, 200, and 350°C regardless of irradiation temperature. Irradiation data indicated that most hardening was caused by Fe^{++} and He^{+} and to a smaller extent by H^{+}.

It is interesting to note that although He^{+} has a very small atomic displacement cross section when compared with Fe^{++} (see Fig. 1), it produced almost equivalent hardening as Fe^{++}. Microstructural evidence indicated that a high number density of small loops and bubbles was produced by He^{+}, which would have contributed to the hardening. Radiation induced defects including black dots, interstitial loops, network dislocations, precipitates, bubbles, and microvoids are considered to be strong barriers and contribute to hardening as well as embrittlement [10-12]. There is evidence that helium can also contribute to hardening by over-pressurized helium bubbles punching out prismatic dislocation loops [13], by promoting the formation of interstitial loops due to the retention of corresponding excess interstitials during the process of helium-vacancy clustering [14], and by direct pinning of dislocations by helium bubbles [15]. In the present study, a few large helium bubbles were observed along grain boundaries, but overall grain boundary bubble distribution and their sizes were similar to those in the matrix. It is thus expected that grain boundary weakening by helium bubbles may not cause any serious problems for 316LN stainless steel in the NSNS operating temperature range (<200°C), although overall ductility loss and embrittlement by helium are still of concern.

Interestingly, H^{+} produced extremely fine black dots and bubbles. Despite the high number density of defects it produced, H^{+} contributed to hardening only to a small extent. It thus appears that defects need to reach a certain threshold size to act as effective barriers to dislocation movement. Although diffusion of gas atom species in metals is complicated by interactions with defects [16-18], hydrogen is known to diffuse several orders of magnitude faster than helium in fcc metals [18]. However, the apparent formation of hydrogen bubbles observed using TEM suggests that hydrogen embrittlement should be carefully evaluated for NSNS target materials.

In spite of the difference in irradiation temperatures, similar defect structures were developed for 80, 200, and 350°C irradiations. Consequently, this resulted in a similar magnitude of increase in hardness for all three temperatures. This temperature insensitive nature of defect sink strength is an interesting finding because tensile tests show a significant temperature dependence for neutron irradiations in this range [19]. Theoretical calculations based on a kinetic model, however, revealed that interstitial and vacancy cluster strength would become less sensitive to temperature with increasing damage rate because defect supersaturation would dominate over a thermal annealing effect [11].

Contrary to the common perception that bubble coarsening occurs earlier at higher temperatures, in the present study, coarser bubbles and bimodal bubble size distribution were observed at 80°C first, not at 350°C. To understand this phenomena, critical bubble sizes at 80 and 350°C were calculated based on a rate theory model [17, 20, 21]. The theory is based on the physical principle that vacancy-gas atom clusters

Lee H

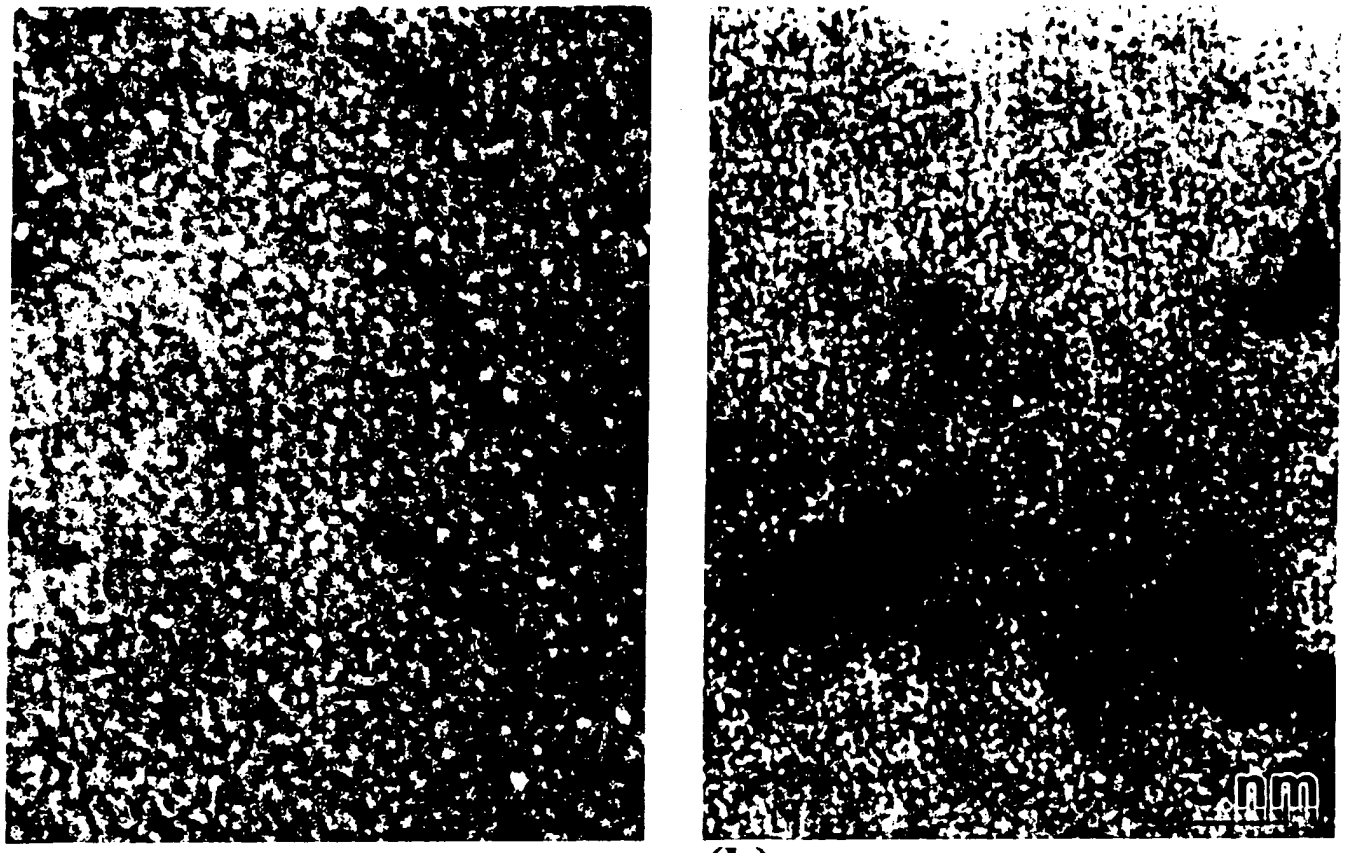

Figure 3: Bubble microstructures for triple ion irradiated specimens irradiated at (a) 80°C, and (b) 350°C.

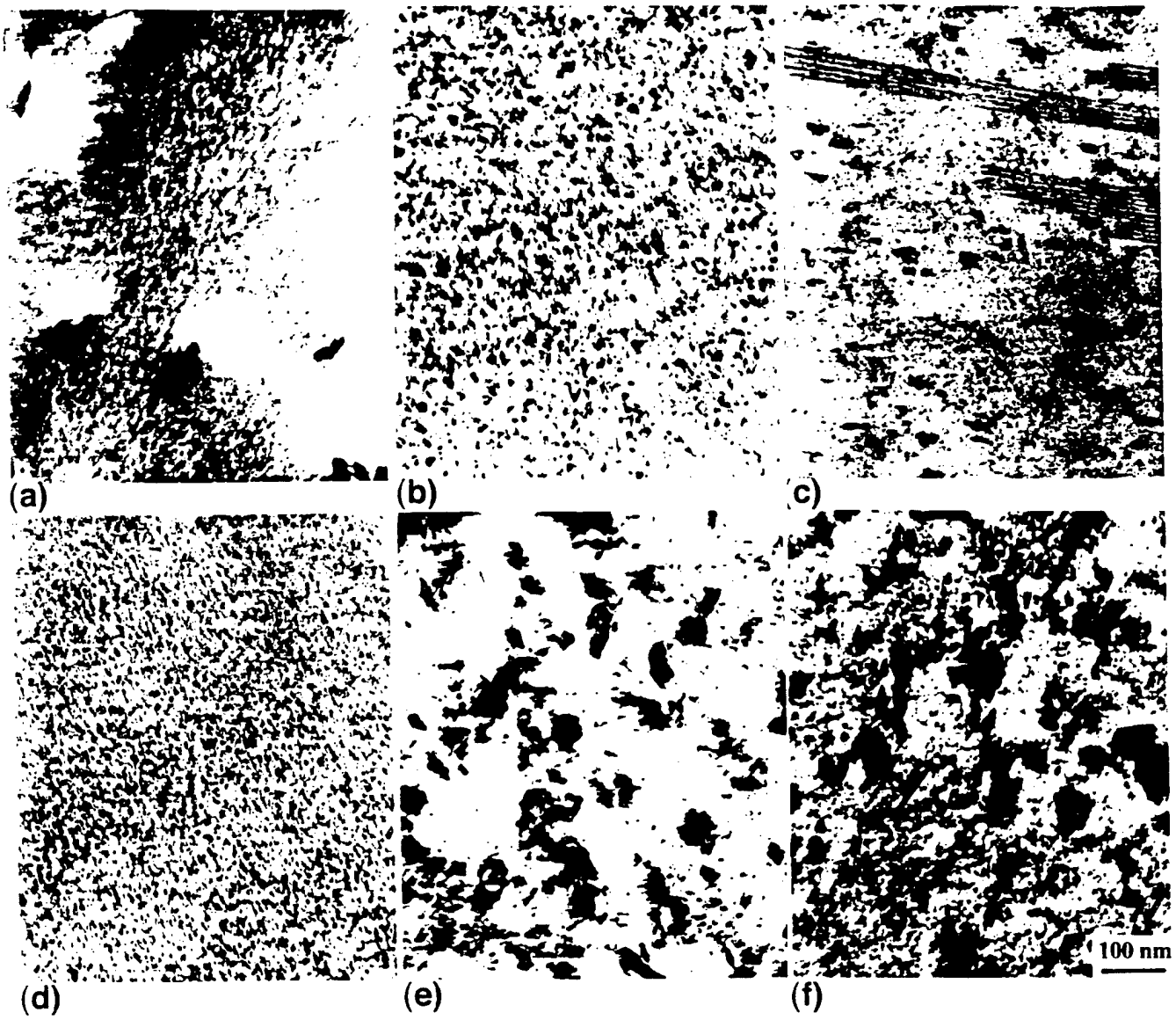

Figure 4: TEM microstructures of dual and single ion irradiated specimens, irradiated at 200°C. The microstructures shown are for (a) H^+ alone, (b) He^+ alone , (c) Fe^{++} alone, (d) He^++H^+ , (e) Fe^{++} + H^+ and (f) Fe^{++} + He^+.

Table IV Summary of Defect Types in Single, Dual, and Triple Beam Irradiated Specimens at 200°C*

3.5 MeV Fe^{++} | 360 keV He^+ | 180 keV H^+						
H^+	He^+	Fe^{++}	H^++He^+	H^++ Fe^{++}	He^++Fe^{++}	H^++He^++Fe^{++}
black dots (<1 nm)	black dots tiny loops (~10 nm)	black dots faulted loops (~50 nm)	black dots coarse dots (~5 nm)	black dots faulted loops (~40 nm)	black dots faulted loops + unfaulted (~70 nm) line segments	black dots unfaulted loops (~30 nm)

*All irradiations produced bubbles when He and/or H ions were implanted.

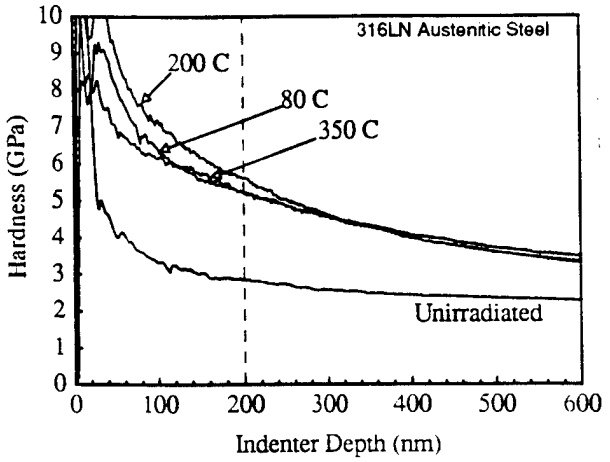

Figure 5: Hardness values of triple ion bombarded specimens irradiated at 80, 200, and 350°C compared with unirradiated material hardness.

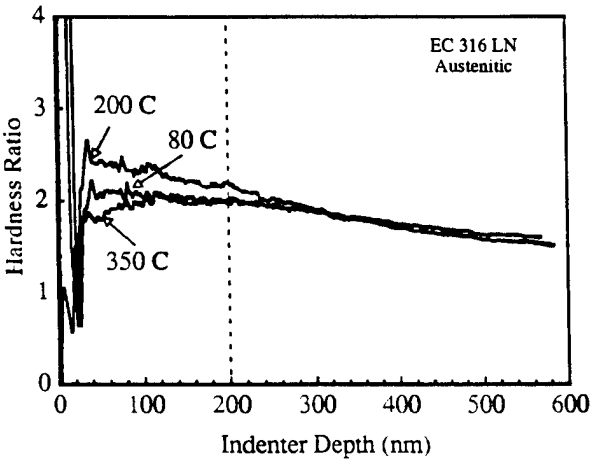

Figure 6: Hardness values of triple ion irradiated specimens normalized to unirradiated hardness value.

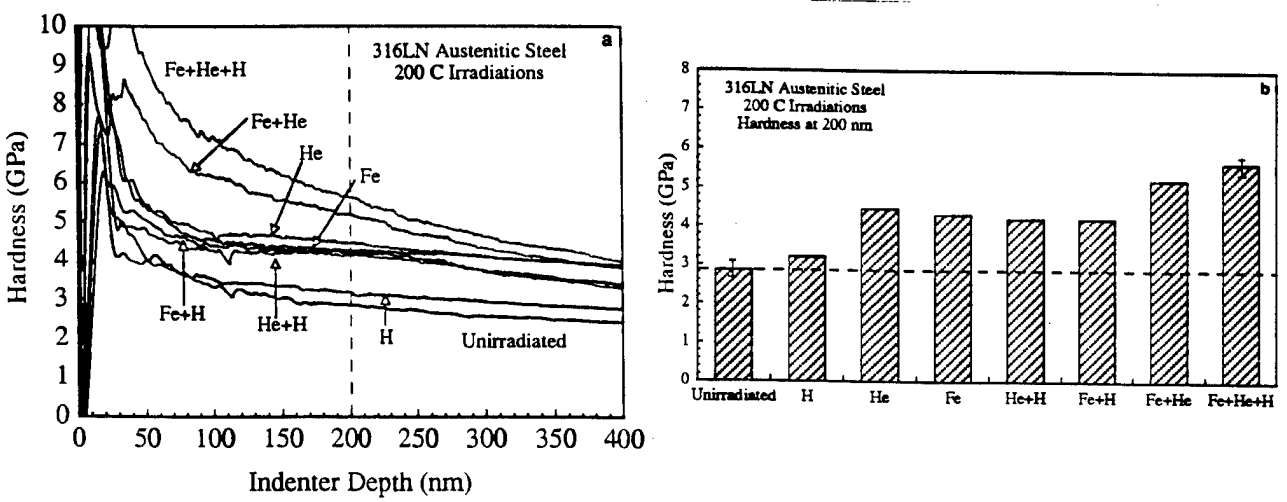

Figure 7: Hardness values as a function indentation depth for 200°C irradiations using triple, dual and single ions (a) and comparison of hardness values at 200 nm depth (b).

do not grow by a vacancy driven mechanism until a critical number of gas atoms are clustered or the gas pressure is built up to a critical level. Thermal emission prevails over absorption of vacancies when bubble size is smaller than a certain size. Calculations of critical quantities in the rate theory formulation require knowledge of materials parameters, irradiation variables, and microstructural information. The detailed theoretical model can be found in references [17, 20, 21]. The results of the calculations are shown in Figure 8 and the material parameters used in the calculation are summarized in the Figure 8 caption. The use of these material parameters has been well justified previously [22], although precise material parameters are unknown. Fortunately, when point defect absorption is controlled by absorption at sinks, the outcome of the calculated values are determined by the dominant sink strength (here, the bubbles), and the use of a wide range of material parameter values do not alter the calculations greatly. It is important to realize that since there are some uncertainties in microstructural and material parameters used in the calculations, the theoretical analysis presented here is intended to be qualitative only. The calculations, however, clearly show that there exists a fundamental physical basis as to why bimodal bubble distribution could occur earlier at 80°C than at 350°C.

During irradiation, bubbles nucleate and grow by forming vacancy-gas atom complexes as they accumulate gas atoms. When bubbles exceed a certain critical size or accumulate a certain number of gas atoms, they can grow inexorably by a vacancy or bias driven mechanism without any further assistance of gas atoms. This demarcates bubble sizes below and above the critical size, thus resulting in a bimodal bubble distribution. Numerous examples of a bimodal bubble distribution are documented in Ref. [17]. Figure 8 compares the calculated critical (r*) and average (r) bubble radii as a function of dose or accumulated helium concentration. As bubbles grow by accumulating gas atoms and vacancies, a bias driven growth sets in when a bubble radius (r) exceeds a critical radius (r*). The results show that a bias driven bubble growth was initiated earlier at 80°C than at 350°C, namely at a helium levels of 8,692 and 9,470 appm, respectively. This was mainly due to the smaller r* at lower temperature, 0.13 nm at 80°C compared to 0.3 nm at 350 °C. This is in agreement with the experimental findings. For materials subjected to irradiation, bias driven void swelling is one of the major concerns. Under NSNS conditions, however, swelling is not expected to impose any serious problem because the calculated bubble growth rate at 80°C was extremely low (~5×10^{-22} m/s).

The hardness data nonetheless suggest that ductility loss and embrittlement could be of concern for long term applications of target materials in the NSNS spallation environment, particularly where cyclic pressure pulses and thermal shocks are expected. Although there is relatively little data for materials performance in spallation environments and none for NSNS conditions, neutron irradiation data suggest that uniform elongation would drop below 10% after 10 dpa for austenitic alloys in the 25 - 400°C range but their strain to necking would be retained above 5% except near 330 ±50 °C [23]. Since the NSNS is expected to operate below 200 °C, austenitic steel may be used below 10 dpa. In this study, however, the employed dose was 50 dpa, and the similar hardness increases observed at all three temperatures suggest that yield strength may have attained the highest level at this dose. At this time, it is not known at what dose level hardness values would saturate. Besides, there is no data for the effects of helium and hydrogen at such high concentration levels expected in the NSNS. Further studies are clearly needed.

Most neutron irradiation data has been acquired under steady irradiation conditions. On the other hand, the NSNS is expected to operate in a pulsed mode with 1 μs proton pulses at 30-60 Hz frequency. During the pulse the instantaneous damage rate is expected to reach up to ~10^2 dpa/s. Point defect concentration buildup during the "beam-on" period and their decay during the "beam-off" period would affect point defect clusterings, the evolution of defect microstructure such as black dots, loops, dislocations, and bubbles, and consequently the mechanical properties.

In a previous study, pulsed single (4 MeV Ni^{2+}) and dual (Ni^{2+} , He^{+}) ion beam irradiations of a Ti-modified austenitic alloy were conducted at 675°C with an approximately equal beam on/off period from 10^{-5} to 60 s [24]. In that work, it was found that the interstitial loop growth rate was lowest during the pulse period which corresponded roughly to the calculated vacancy lifetime of 10^{-3} and 10^{-1} s for helium-implanted

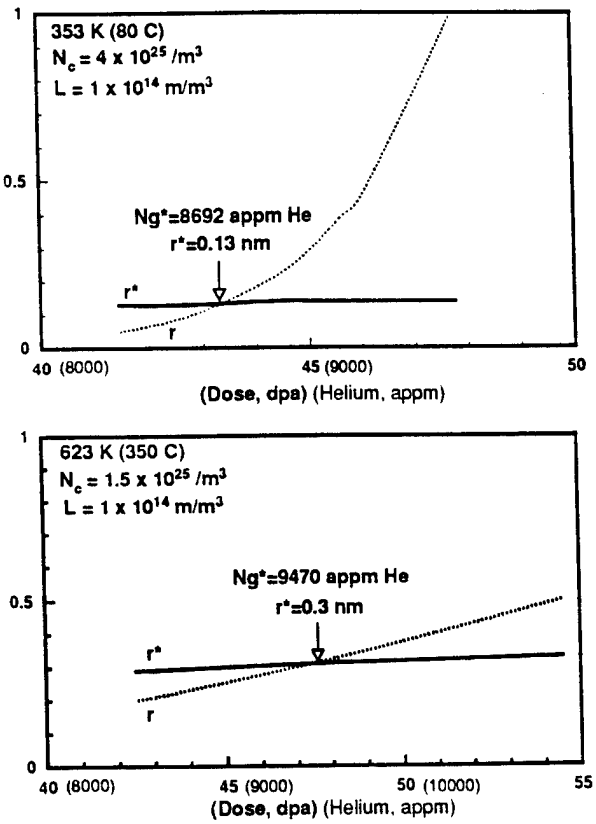

Figure 8: Average (r) and critical (r*) bubble sizes as a function of dose or injected helium concentration. The microstructure parameters and irradiation temperatures are shown in the figures. The parameters used in this computation are displacement damage rate $G=1\times10^{-3}$ dpa/s, vacancy diffusivity pre-exponential $D_v^o=1\times10^{-6}$ m^2/s , interstitial diffusivity pre-exponential $D_i^o=1\times10^{-6}$ m^2/s, vacancy migration energy E_v^m= 1.2 eV, interstitial migration energy E_i^m=0.15 eV, vacancy formation energy E_v^f=1.6 eV, vacancy formation entropy S_v^f=1.29x 10^{-4} eV/K, Bias=0.05, and surface energy γ=1.5 J/m^2.

and helium-free material, respectively, consistent with theoretical predictions for the effects of pulsing. In the NSNS, the beam-off period would be relatively longer compared to beam-on period, thus allowing more time for defect annealing. This may help in extending the lifetime of the target materials. On the other hand, the sluggish defect kinetics at low temperatures (<200°C) may offset the beneficial effects of annealing. Further studies are planned to understand the effects of pulsing.

Conclusions

Materials performance in a spallation neutron source environment has been investigated by studying hardness changes and TEM microstructures for a candidate 316LN austenitic alloy. The alloy was irradiated with single, dual, and triple ion beams using 3.5 MeV Fe^{++}, 360 keV He^{+}, and 180 keV H^{+}. Irradiations were conducted at 80, 200, and 350°C. An Fe^{++} dose of 50 dpa was used, and injected helium and hydrogen levels were 10,000 appm and 50,000 appm, respectively.

TEM examination revealed that predominant radiation-induced defects were black dots, dislocation loops, and bubbles. Single ion beam results showed that H^{+} produced fine black dots and bubbles, He^{+} produced small loops as well as black dots and bubbles, and Fe^{++} produced black dots and larger loops. Comparison of single, dual, and triple beam irradiated microstructures indicated that hydrogen had a tendency to refine the loop defect microstructure. Comparison between microstructure and hardness data indicated that irradiation induced hardening occurred mainly by defects produced by Fe^{++} and He^{+}. Hardening by H^{+} was significantly less effective compared to the hardening caused by He^{+} or Fe^{++}. The hardness also showed a similar magnitude of increase from ~3 GPa to ~5.5 GPa regardless of the irradiation temperature. This temperature insensitive nature of hardness was explained by appealing to a theoretical model which suggested the radiation-induced defect microstructure would be insensitive to temperature at a high damage rate condition, because high defect supersaturation overshadows the thermal annealing effect at low irradiation temperatures.

An extremely high bubble number density was observed at all temperatures for triple beam irradiation. The bubble number density appeared to decrease with increasing irradiation temperature. Interestingly, however, a bimodal cavity distribution was observed at 80°C, but not at 350°C. Calculations based on a rate theory model indicated that the critical bubble sizes were ~0.13 and ~0.3 nm at 80 and 350°C, respectively. Therefore bias driven bubble growth initiated earlier at 80°C, consistent with the experimental findings. In spite of bias driven growth, swelling was insignificant because of slow bubble growth rate at low temperatures.

Under the NSNS pulsed mode irradiation, defect annealing may occur during the "beam-off" period. This may extend the service lifetime. Further studies based on beam on/off effects are planned. Overall, the present ion irradiation studies suggest that the most important concern in the spallation target material is ductility loss by radiation-induced hardening and embrittlement caused by hydrogen and helium. Based on neutron irradiation data, austenitic steel may be used below 10 dpa for target applications. At this time, very little is known about embrittlement effects caused by hydrogen and helium at such high concentration levels expected under NSNS conditions. It is also not known how hardening would be affected by cyclic stresses due to thermal and hydraulic shocks. These observations clearly suggest that further studies are needed to provide in-depth understanding.

Acknowledgments

This research was sponsored by the Division of Materials Sciences, U.S. Department of Energy, under contract No. DE-AC05-96OR22464 with Lockheed Martin Energy Research Corporation. The authors would like to thank Dr. Roger Stoller and Dr. Janet Robertson for technical review of the manuscript.

References

1. L. K. Mansur and H. Ullmaier, Proceedings of the International Workshop on Spallation Materials, Oak Ridge, Tennessee, April 23-25, 1996.
2. National Spallation Neutron Source Conceptual Design Report, NSNS/CDR-2/V1 and V2, Oak Ridge National Laboratory, U.S. Department of Energy, May 1997.
3. M. B. Lewis, W. R. Allen, R. A. Buhl, N. H. Packan, S. W. Cook, and L. K. Mansur, *Nucl. Instrum. Methods*, **B43** (1989) 243.
4. J. F. Ziegler, J. P. Biersack, and U. Littmark, "The Stopping and Range of Ions in Solids, Pergamon Press (1985).
5. ASTM E521-89, Neutron Radiation Damage Simulation by Charged-Particle Irradiation, ASTM Book of Standards **12.02**, (1990).
6. W. C. Oliver and G. M. Pharr, *J. Mater. Res.*, **7** (1992) 1564.
7. E. H. Lee, Y. Lee, W. C. Oliver, and L. K. Mansur, *J. Mater. Res.*, **8** (1993) 377.
8. A. K. Bhattacharya and W. D. Nix, *Int. J. Solids Structures*, **24** (1988) 1287.
9. P. B. Johnson and D. J. Mazey, *Nature*, **276** (1978) 595.
10. A. L. Bement, Jr., Proc. On the Strength of Metals and Alloys (ASM, Metals Park, 1970) 693.
11. R. E. Stoller, "Effects of Radiation on Materials," 16th Int. Symp., ASTM STP 1175, A. S. Kumar, D. S. Gelles, R. K. Nanstad, and E. A. Little, Eds., American Society for Testing and Materials, Philadelphia (1993) 394.
12. M. L. Grossbeck, P. J. Maziasz, and R. F. Rowcliffe, *J. Nucl. Mater.*, **191-194** (1992) 808.
13. H. Trinkaus, *Radiation Effects*, **78** (1983) 189.
14. K. Farrell, R. W. Chickering, and L. K. Mansur, *Phil. Mag. A*, **53** (1986) 1.
15. E. H. Lee, N. H. Packan, M. B. Lewis, and L. K. Mansur, *Nucl. Mater. Meth.*, **B16** (1986) 25.
16. D. J. Reed, *Radiation Effects*, 31(1977)129.
17. L. K. Mansur, E. H. Lee, P. J. Maziasz, and A. F. Rowcliffe, *J. Nucl. Mater.*,. **141-143** (1986) 633.
18. V. Sciani and P. Jung, *Radiation Effects*. **78** (1983) 87.
19. J. E. Pawel, A. F. Rowcliffe, G. E. Lucas and S. J. Zinkle, J. Nucl. Mater., 239 (1996) 126-131.
20. L. K. Mansur, Nuclear Technology, 40 (1978) 5.
21. L. K. Mansur, Chapter 8 in "Kinetics of Nonhomogeneous Process," G. R. Freeman ed., John Wiley & Sons (1989) 377.
22. E. H. Lee and L. K. Mansur, Met. Trans. A, 21 (1990) 1021.
23. J. E. Robertson, I. Ioka, A. F. Rowcliffe, M. L. Grossbeck, and S. Jitsukawa, "Effects of Radiation on Materials," 18th Int. Symp., ASTM STP 1325, R. K. Nanstad, M. L. Hamilton, F. A. Garner, and A. S. Kumar, Eds., American Society for Testing and Materials, Philadelphia (1997).
24. E. H. Lee, N. H. Packan, M. B. Lewis, and L. K. Mansur, Nucl. Instrum. Meth. Phys. Res. B16 (1986) 251.

Lee 9

Report Number (14) CONF-970201--31

Publ. Date (11) 199709

Sponsor Code (18) DOE/ER, XF

UC Category (19) UC-400, DOE/ER

DOE